Picosecond photofragment spectroscopy. II. The overtone initiated unimolecular reaction H2O2(v OH=5)→2OH

Norbert F. Scherer and Ahmed H. Zewail

Citation: The Journal of Chemical Physics **87**, 97 (1987); doi: 10.1063/1.453529
View online: http://dx.doi.org/10.1063/1.453529
View Table of Contents: http://scitation.aip.org/content/aip/journal/jcp/87/1?ver=pdfcov
Published by the AIP Publishing

Picosecond photofragment spectroscopy. II. The overtone initiated unimolecular reaction $H_2O_2(v_{OH}=5)\rightarrow 2OH$

Norbert F. Scherer and Ahmed H. Zewail
Arthur Amos Noyes Laboratory of Chemical Physics,[a] *California Institute of Technology, Pasadena, California 91125*

(Received 9 December 1986; accepted 11 February 1987)

This paper, second in the series, reports on the picosecond time-resolved photofragmentation of the overtone ($v_{OH}=5$) initiated reaction: HOOH + $h\nu\rightarrow$2OH. The hydrogen peroxide is initially excited by way of a picosecond laser pulse to the fourth overtone level of the OH-stretch local mode. The subsequent unimolecular reaction behavior is obtained by monitoring the laser-induced fluorescence, caused by the picosecond probe–pulse electronic excitation of the OH radical photoproduct (in a given rotational state). The two pulses are scanned relative to one another in time thereby mapping out the product yield for the given delay-time interval. The resultant product formation behavior is found to be nonexponential, and may be modeled as a biexponential rise. Furthermore, the quasibiexponential behavior is sensitive to the exact excitation wavelength—slight variations of which result in large changes in the two time constants and the relative amplitudes of the fast and slow components. These experiments give direct evidence for the inhomogeneous nature of the overtone transition on the picosecond time scale, and provide the dissociation rate contribution to the homogeneous width (0.05–0.15 cm^{-1}). The apparent width for the main band feature is about 200 cm^{-1}. The rate of product formation (magnitude and form) is interpreted in terms of *statistical* and *nonstatistical* theories. The limitations of the applicability of each model is discussed. The fluctuations of the fitting parameters as a function of excitation wavelength may be simulated by a statistical model which considers all possible discrete optical transitions within the simulated laser bandwidth and the details of product formation from each state. For a nonstatistical interpretation, the biexponential form reflects a division of the vibrational phase space, and this is discussed in the spirit of a kinetic model. Finally, experimental results are reported for direct UV initiated photofragmentation. The observed dynamics indicate that a very different type of potential surface (repulsive) is involved, in contrast to the overtone initiated dissociation, which takes place on the ground state surface.

I. INTRODUCTION

The highly state-selective nature of optical overtone excitation encourages the possibility of the study of state-to-state reaction dynamics and bond-selective chemistry.[1] The specificity in the initial state creation results from rigorous transition selection rules in the excitation process. In contrast to unimolecular reactions which proceed via mechanisms involving internal conversion or intersystem crossing (see e.g., Ref. 2), local-mode (LM) excitation[3] of CH or OH oscillators provide a "site selective" method of depositing the energy in a given bond on the ground potential energy surface. Such a well defined initial state should allow for the detailed examination of the effect of intramolecular vibrational energy redistribution (IVR), from the LM into the reaction coordinate, on the dynamics of reaction. The trying aspect of such experimental studies stems from the small absorption cross sections ($\sigma\leqslant 10^{-23}\,cm^{-2}$) for transitions to those overtone levels (e.g., fourth, fifth, or higher) which are sufficiently energetic to obtain molecular dissociation (typically 40–60 kcal/mol). The consequent small excited molecule population makes the study of intramolecular dynamics and reaction rates difficult.

Following the spectroscopic measurements of the linewidth of LM states (typical 100–150 cm^{-1} in large molecules), it became clear that time-resolved study of the (picosecond) dynamics of such states are necessary. The need for direct measurements of the time evolution stems from the realization that the linewidth of LM states may not be directly related to the true rate(s) of energy relaxation and/or reaction out of such states. This is because dephasing and inhomogeneous broadening could contribute significantly to the linewidth.[4] Many attempts were made in this laboratory to measure the picosecond dynamics of LM states but without success. Our recent report[5] on the overtone initiated dissociation of hydrogen peroxide is the first successful picosecond time-resolved overtone experiment to directly obtain such information. The reaction studied is

$$HOOH(v_{OH}=5 \text{ excitation})\rightarrow 2OH.$$

The method, as depicted in Fig. 1, may be briefly described as a picosecond laser pulse exciting the molecule to the fourth overtone ($v_{OH}=5$) while a second (ps) pulse interrogates the OH radical reaction product formed in a specific rovibrational state. The OH laser-induced fluorescence (LIF) signal is monitored as a function of the relative

[a] Contribution No. 7514.

 0021-9606/87/130097-18$02.10

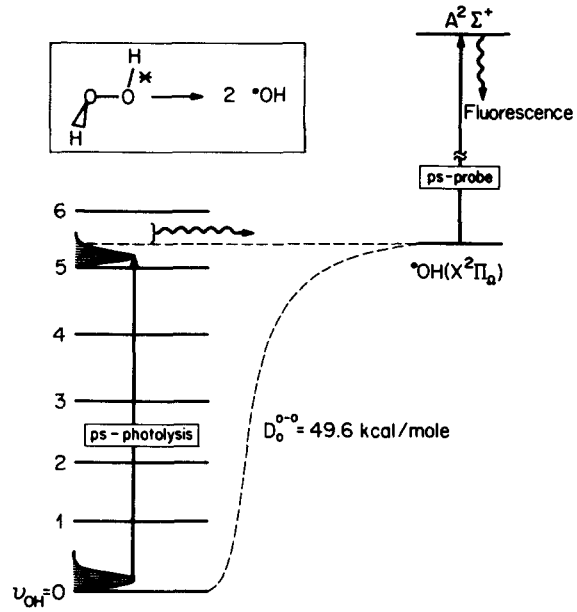

FIG. 1. The schematic of the picosecond overtone pump/OH LIF probe method. A picosecond pump pulse prepares the HOOH in the fourth overtone level of the OH stretching mode. Only states in the tail of the thermal distribution are energetic enough to dissociate. Intramolecular energy redistribution transfers the excitation + thermal energy to the reactive coordinate. The subsequent dissociation forms the OH radical product in various rotational states. A picosecond probe pulse excites the OH radical via the $^2\Sigma \leftarrow {}^2\Pi$ electronic transition. The resultant OH-LIF signal is proportional to the amount of ground state OH product in the specific state probed by the laser. The pump and probe laser pulses are scanned in time.

delay between the excitation and probe pulses. This development has afforded us with the capability to directly monitor the unimolecular reaction rates. The rates, taken in conjunction with the previously determined product state distributions,[6] should provide critical tests for theories of unimolecular reaction dynamics. Since the initial excitation is of the LM of the OH stretch and the reaction involves another coordinate, i.e., breaking the O–O bond, this motion of the internal energy implies that these studies are relevant to the IVR process and to the dynamics of the (ro-) vibrational phase space. The measured rate of reaction provides, by way of the Fourier transform, the contribution of the unimolecular dissociation to the homogeneous linewidth of the given transition. The apparent width[6] for this fourth overtone level is approximately 200 cm^{-1}.

The aesthetic appeal of the HOOH system results, in part, from it being a tetraatomic species for which there are few enough degrees of freedom such that the potential exists for making detailed theoretical/experimental comparisons. Also, prior to our work, there exist the results of numerous spectroscopic[7] and structural[8] investigations of hydrogen peroxide which are valuable to the present study. The types of studies which are most salient to the present work include elucidation of the (OH-stretch) ground state torsional potential,[9] some spectral assignments of the fourth overtone predissociation features by Crim's group,[6(b)] and photodissociation studies of the higher lying (repulsive) electronic states by Bersohn's group and by Klee *et al.*[10] There is an implicit simplification in coming to understand the dynamics of overtone-initiated reactions since the dissociation proceeds exclusively on the ground electronic surface and correlates to the lowest electronic configuration of the OH radical products.[11] Surface crossing and the associated non-Born–Oppenheimer wave functions are not an added complication to the interpretation of experimental results. Classical trajectory studies by Uzer, Hynes, and Reinhardt[12] have provided an enlightening description of a method by which energy redistributes from the LM to the reaction coordinate on the ground state surface of HOOH.

A practical appeal has to do with the reasonably low electronic ground state dissociation energy ($D_0 = 49.6$ kcal/mol),[13] which allows direct overtone pumping of the OH stretching mode facilitating studies of the ensuent reaction. Such excitation energies are readily accessible to amplified picosecond laser systems, thus enabling the measurements to be made. The product states of OH($X^2\Pi_\Omega$) fragment can also be probed using amplified picosecond pulses at UV wavelengths.

The remainder of this paper is structured in the following manner. A detailed description of our method for extension of the time domain for the overtone-pump LIF-probe technique and its application to the HOOH system is given in Sec. II. This will be followed by a presentation of some spectroscopic phenomenology (Sec. III) and the experimental results in Sec. IV which manifest the effect of the variation of the initially prepared state(s) on the subsequent reaction dynamics. Finally, in Sec. V we discuss the significant experimental observations of the product quasibiexponential buildup and the nonmonotonic behavior of the rate of molecular dissociation with respect to laser excitation energy. The results will be compared with statistical rate calculations and nonstatistical reaction theories. This will include an elaboration on the implications of conformity of the calculated results to the room temperature experimental data.

II. EXPERIMENTAL

The experimental arrangement essentially consists of four parts: (A) picosecond pulse generation, amplification and characterization; (B) the optical interferometer, gas cell, and laser induced fluorescence (LIF) detection scheme; (C) the HOOH sample and OH resonance calibration; and (D) the details of the methods used for signal acquisition and averaging, and data (also called transient) processing.

A. Two-color picosecond pulse generation and characterization

The picosecond pulses used in this study are produced by the synchronously pumped dye laser system depicted schematically in Fig. 2. The pulse initiation source is a Nd:YAG laser which is mode locked using a stabilized[14] acousto-optic modulator as the loss modulation element. The 532 nm output of the YAG laser (82 MHz rep. rate, < 80 ps pulses, 800 mw power, 10 nJ/pulse) synchronously pumps two cavity-length matched R6G dye lasers. The first dye laser (DL1) contains a three-plate birefringent filter as the tuning element, while the second dye laser (DL2) utilizes an identical three-plate birefringent filter as well as a

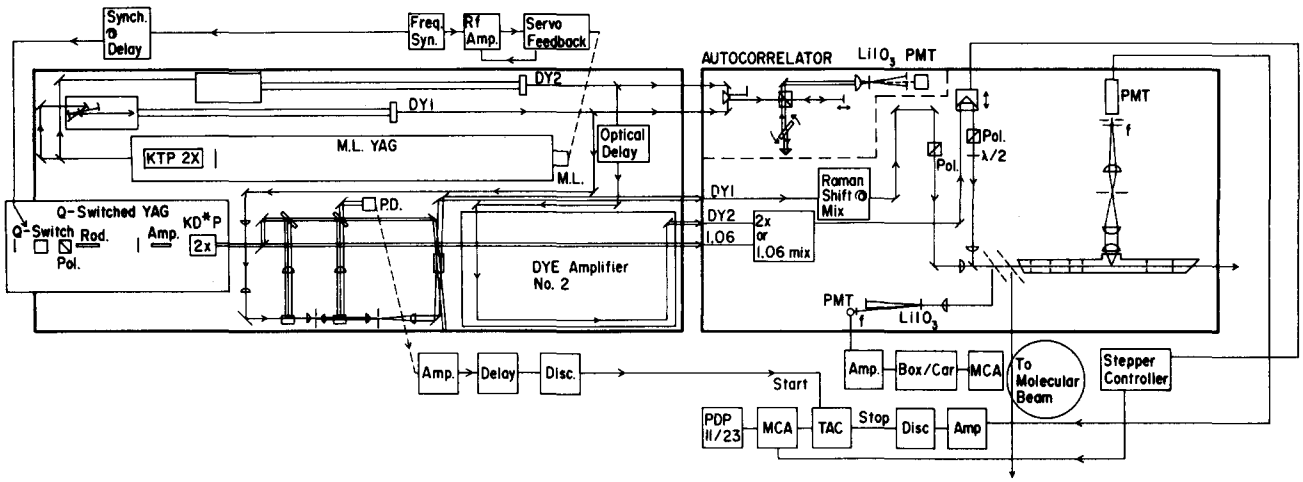

FIG. 2. The experimental arrangement. Three essential parts: (i) Laser system, oscillator, amplifiers, real-time pulse diagnostics; (ii) interferometer arrangement; (iii) gas phase bulb and the molecular beam apparatus. The abbreviated terms are explained in the text. The heavy borders represent the outlines of the optical tables. Amplifier 2 is essentially the same as amplifier number 1. The arrow labeled "to molecular beam" is in reference to the preceeding and subsequent papers in this series, and for peroxide experiments in progress.

fine étalon (40 GHz cw bandpass) as tuning elements. Output couplers of 30% transmissibility are used in both lasers to ensure good pulse formation via mode competition.[15] The output of the first dye laser (82 MHz, 6–7 ps Gaussian pulses, 50 mw average power, 1 nJ/pulse, approximately transform limited) is amplified in a three-stage (home-built) pulsed dye amplifier with a Q-switched Nd:YAG laser (20 Hz, 3.5 ns pulse, 200–250 mJ/pulse at 532 nm) as a pump source. The second dye laser's output (11 ps Gaussian pulses, 40 mw average power, approximately transform limited) is amplified in a separate, but essentially identical, three-stage dye amplifier pumped by the same Q-switched laser. The synchronization of the YAG Q switching and the arrival of the dye laser picosecond pulse at the amplifiers is suitably adjusted for maximum amplified power by way of electronic and optical delays. Each dye amplifier consists of two transversely pumped dye stages and a final counter propagating longitudinally pumped dye cell. The cells are isolated by spatial filters to discriminate against amplified spontaneous emission and to facilitate wavelength tunability. The optics design maintains the TEM_{00} mode of the synch-pump laser through the amplifier. In the third amplification stage, the longitudinal pumping causes the output mode to take on the "doughnut" transverse mode of the Q-switched laser. The picosecond beam diameter is increased in each succeeding dye stage to prevent nonlinear distortions (e.g., dielectric breakdown, self-phase modulation) from broadening the pulse in time or frequency. The linear group velocity dispersion, caused by the wavelength dependent change in the index of refraction of the optics and dye medium, contributes approximately 2 ps (assumed Gaussian), in convolution with the input pulse width, to the time duration of the amplified pulses. The output pulses of the dye amplifiers (20 Hz, 6.6 or 11.2 ps, 0.5 mJ/pulse) are injected into the optical arrangement for the delay line and are split off for pulse characterization.

The oscillator dye laser pulses and the amplified pulses are analyzed in time using background-free second harmonic generation (SHG)[16] and in frequency by monitoring the bandwidth. A real-time autocorrelator is used to aid in the adjustment of the dye laser cavity lengths and is also used to obtain signal-averaged autocorrelations for pulse analysis. This home-built spinning-block design also allows for the measurement of the cross correlation of the two dye lasers. The amplified pulse autocorrelations are acquired using a stepper motor variable delay interferometer which makes repetitive-scan signal averaging possible. It is found that the oscillator and amplified pulses are essentially equivalent in the present laser configuration, that is, the amplifier is not (appreciably) broadening or distorting the picosecond pulses in time or frequency. The acquired autocorrelations are deconvoluted with symmetric Lorentzian, Gaussian, or sech model functions for the pulse duration using a nonlinear least-squares fitting routine. It should be noted that such symmetric model functions are only a convenient approximation to the true pulse shape.[17] If a log plot of the autocorrelation data shows evidence for the existence of another component, an additional deconvolution is performed for the noise burst model[18]–coherence spike.[19] This precaution was unnecessary, however, for the present experimental arrangement of tuning elements. The oscillator and amplified pulse cross correlations may be obtained with the same experimental arrangements and their measurement involves only minor alignment adjustments. These cross correlations are deconvolved using the respective autocorrelation information and a symmetric model function to account for the pulse jitter.[20] It may be noted that the amplification process does not adversely affect the modeled jitter.

Figure 3 displays typical auto- and cross correlations obtained by background free sum frequency generation. The cross correlation is deconvoluted with a 6.6 ps Gaussian pulse (obtained from the autocorrelation of DL1) and yields a 11.5 ps Gaussian component. This second contribution is very similar to the 11.2 ps Gaussian pulse width obtained form the autocorrelation of the second dye lasser. The contribution from the cross-correlation jitter is <3 ps in this

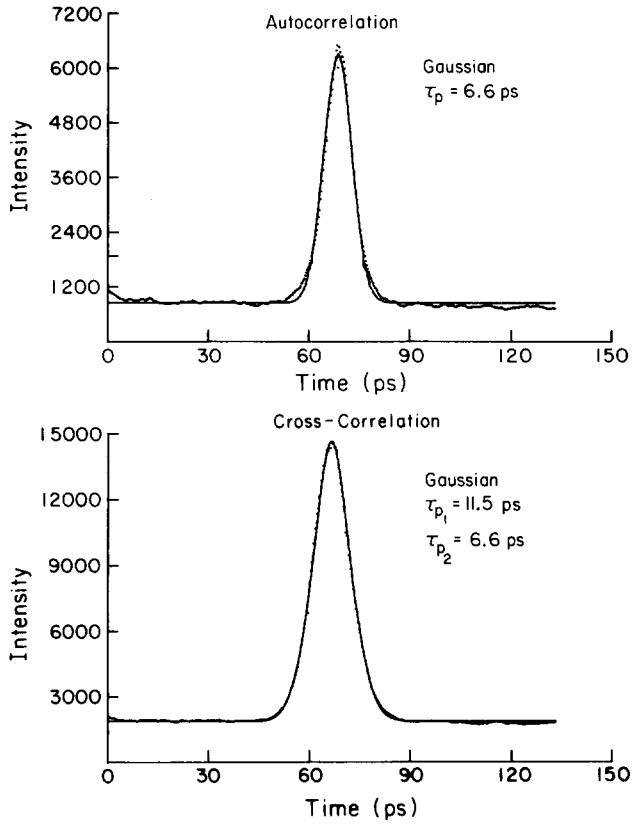

FIG. 3. Auto- and cross correlations of the amplified pulses. The correlation functions are generated by sum frequency generation, as seen in the lower portion of Fig. 2, utilizing the scanning interferometer arrangement of Fig. 2. The fitted autocorrelation pulse width is $\tau_p = 6.6$ ps FWHM Gaussian, cross correlation fitted pulse widths (Gaussian) are $\tau_{p_1} = 6.6$ ps and $\tau_{p_2} = 11.5$ ps which is very similar to the autocorrelation of DY2 (not shown) of 11.2 ps. The ratio of amplitudes for the contributions to the cross is equal to 1.

case. This value is small in comparison to the pulse widths, and is perhaps also (partially) due to the assumption that the pulse may be represented by a symmetric model function.

Bandwidth measurements are performed using a Spex 0.75 m monochrometer, which has 0.25 cm^{-1} spectral resolution at 600 nm for 20 μm slits. The pulse bandwidths are fit with a Gaussian functional form and are deconvoluted for the monochrometer resolution. It is found that the oscillator and amplified bandwidths for DL1 are equivalent and are 2.6 cm^{-1} at 607.5 nm while the bandwidth of DL2 is 2.8 cm^{-1} at 303.75 nm. This gives a pulse duration–bandwidth product of 0.50 for DL1, as compared to the transform limit of 0.441 for minimum uncertainty (Gaussian) pulses.[16]

B. Pump–probe arrangement

1. Visible pump–UV probe

The optical scheme, as represented in the remaining portion of Fig. 2, consists of an optical interferometer arrangement in which the amplified outputs of DL1 and DL2 enter the fixed and variable delay arms, respectively. The pump beam of 200 μJ pulse energy at the sample is focused to a 0.25–0.5 mm spot size. The probe light (DL2) is generated using a KDP crystal to frequency double the laser fundamental. The second harmonic beam enters the variable delay arm of the interferometer, which (usually) contains a beamsplitter, a corner cube on a stepper motor actuated translation stage and a zero degree retroreflector to double pass the beam through the scanning corner cube. This double pass arrangement facilitates long scans (2.5 ns) and ensures beam positioning accuracy when the arrangement is properly aligned. Figure 2 shows an arrangement for a single-pass through the corner cube. This is done for the purpose of enhanced visual clarity, and is an alternative experimental scheme. The delayed beam passes through the beamsplitter, is analyzed with a Glan–Taylor polarizer and is rotated by a half-wave plate. This optical arrangement allows making the relative pump–probe polarizations parallel or perpendicular for the various measurements. Placing the waveplate after the analyzer allows polarization changes to be made without significantly disturbing the beam overlap. This arrangement obtains extinction ratios of $\geqslant$20:1. The probe beam is focused separately from the pump beam to a diameter of 0.25–0.5 mm and is attenuated to $<0.25\,\mu$J pulse energy. The beams are recombined with a dichroic reflector, are carefully adjusted to be collinear and propagate through the HOOH/LIF cell. Independent focusing enables one to position the pump and probe beam waists at the fluorescence cell viewing window and match the spot sizes. Chromatic aberation of these two (infinite conjugate ratio) beams does not allow one lens to do this effectively while maintaining a reasonable spot size.

The system response function is obtained by generation of the difference frequency signal[21] between the pump and probe beams under time delay conditions identical to those for a given experimental transient. The collinear beam condition employed satisfies[22] a k vector matching condition of the form $\Delta\bar{k} = 0 = \bar{k}_1 + \bar{k}_2 - \bar{k}_3$, where $\bar{k}_3$ represents the wave vector for the beam from DL2, $\bar{k}_1$ is that from DL1, and $\bar{k}_2$ is that associated with the difference frequency beam. This light is monitored slightly off-axis of the DL1 and DL2 beams since it cannot be preferentially selected by spectral or polarization discrimination methods. The extreme divergence of this beam results from the chromatic aberation of focusing into the nonlinear crystal with a single lens. The same interferometer as described above is used to generate the pump–probe cross correlations. The changes in the optical arrangement involve rotation of the half-wave plate and analyzer to produce perpendicular relative polarizations of the beams, appropriate attenuation of the pump and probe beams to avoid damaging the nonlinear crystal while maintaining the same relative time delay (i.e., time zero is not shifted), and inserting a plane mirror before the sample cell to direct the beams into a 1.5 mm $LiIO_3$ crystal. The difference frequency beam is monitored with a photodiode, and the signal is recorded as the delay-line scans over the identical range as for the corresponding experimental transient. The observed response functions are shorter (in time) than the corresponding cross correlations of the two visible beams since the pulse from DL2 has been frequency doubled. The shape of the second harmonic pulse is proportional to the square of the $\hat{e}$ field, causing the pulse duration (for a trans-

form limited pulse and no group velocity dispersion contribution) to become $\approx\sqrt{2}$ shorter.

2. UV pump–UV probe

An alternative pump scheme was used which involves the same probe arrangement but differs in that the pump wavelength is 282 nm. This is done for the purpose of probing the dissociative electronic state for comparison with the direct overtone excitation scheme. The generation of this light involves inserting a methane Raman shifter in the path of DL1 (along with appropriate focusing and recollimating lenses), mixing the resultant anti-Stokes shifted light with the fundamental frequency in another KDP crystal (sum frequency generation). An appropriate set of dichroic beamsplitters and recombiners send this new pump beam along the fixed delay path of the formerly visible pump beam. Similar overlap and beam waist position criteria to those described above are used for lens and recombiner positioning. The response function for this UV pump scheme is not readily obtainable by difference frequency generation since this entails the detection of 3000 cm^{-1} light—we were not equiped with the necessary (e.g., Ge) detector.

Several other pump–probe schemes are possible—the essential difference lying in the method of generation of the specific frequencies of light required in the particular experiment of interest. The common factor remains the utilization of the scanning delay line interferometer.

C. Sample preparation and signal acquisition

There are several considerations involved in the design of the sample cell. Since HOOH catalytically decomposes on metal surfaces, the construction materials consist exclusively of glass and Teflon. A flowing vapor cell is necessary to replenish the sample in the observation region and to minimize the effects of wall decomposition. A capacitance manometer (MKS Instruments Baratron 222BA) is used to monitor the pressure and thereby regulate the rate of OH quenching[23,24] and ensure that the observed transients are not distorted by an extreme pressure condition. Finally, the cell must be designed to effectively discriminate against scattered laser light, in particular that which is derived from the probe beam. The pump light may be filtered (Corning 7-54) before the PMT detector. The probe light, however, is more troublesome in that the LIF is monitored for the resonance fluorescence—filtering is not possible. Extensive light baffling of the probe light within the cell was a feasible solution. As may be seen in Fig. 2, several black Teflon light baffles are incorporated into the cell.

The OH LIF is detected at right angles through a fused silica viewing window. The emission is collected and collimated with an $f/1$ plano-convex lens and focused with a $f/2$ lens onto a 2 mm slit. The transmitted light is refocused by an $f/1.5$ lens onto a 7.5 mm slit which is located just before the detecting high gain PMT (EMI 9635QB). The several slit aperatures further reduce the amount of scattered laser light and a filter (7-54) in front of the PMT removes essentially all of the visible beam scatter.

The HOOH sample (70%, FMC Corp.) is extensively degassed by repeated freeze–pump–thaw cycles before being used. The pressure in the cell is regulated by adjusting a Teflon needle valve which separates the sample holder from the cell's main body. The cell is actively pumped on (cryotrapped stokes pump) to establish HOOH flow through the fluorescence viewing region to prevent the accumulation of the photo- and wall dissociation products. Tuning into the $A\,^2\Sigma \leftarrow X\,^2\Pi_\Omega$ OH resonance transition of interest is most easily done using a (Bunsen) burner flame as an OH radical source.[24] The dye laser wavelength is adjusted while monitoring the LIF signal from the flame source with a filtered (7-54) PMT (Hamamatsu 1P28a).

The observed photoproduct OH LIF signal level is expected to be low because of several contributing factors; the absorpting cross section for this transition to the fourth overtone ($< 10^{-23}$ cm^2) and the sample number density are small. In addition, the picosecond pulse energy is $\approx 1\%$ that of the nanosecond pulses used in Ref. 6. Therefore, less than one detectable event per laser pulse is anticipated, indicating the suitability of a single photon counting detection scheme. The Q-switched YAG pulse is monitored with a fast photodiode (H.P. 5082-4220), amplified in an inverting amplifier (H.P. 461A), discriminated (Ortec 473A), and used for the start input signal of a time-to-amplitude converter (Ortex 457 TAC). The output of the EMI PMT is amplified (Comlinear CLC100), passes through a 130 ns delay, is fed into a differential discriminator (Ortec 583), and is used as the stop pulse of the TAC. The delay serves to prevent the TAC from registering the scattered light events. The detection window for the TAC is adjusted to be 1 μs (duty cycle: 0.002%) to maximize the number of countable events and still maintain good discrimination with respect to the tube dark counts (< 100 events per second, uncooled). In this detection scheme the signal event rate must be less than the pulse repetition rate to avoid biased sampling problems, therefore, maximum experimental count rates were maintained to < 4 counts per second for this 20 pps laser system. For the case of uncorrelated photon statistics (Poisson), two photon biased sampling events would occur at most 6% of the time.

D. Signal processing

The signal is accumulated in an MCA (Tracor Northern 1706) whose channel advance is synchronized to the variable delay line stepper motor controller. The accumulated transient is transfered to a minicomputer (MDB PDP11/23 +) for storage and further processing. The maximum accumulated signal level in a given channel of the 512 channel memory is typically 250 counts per scan—only one quarter of this consititutes a background signal. Accordingly, a maximum S/N ratio for Poisson noise statistics is 13:1. Some of the experimental noise is systematic causing the S/N ratio to be somewhat less. The transients which are presented herein are data which have been smoothed using a three point Gaussian weighting function. This enhances the transient S/N but has no effect on the fitting parameters.

Transients are fit with a single or biexponential model function of the form

$$S_{\text{trans}} = \int_{-t_1}^{t_2} \{\alpha_1[e^{(-t/\tau_1)}] + \alpha_2[e^{(-t/\tau_2)}]\} \cdot I_{\text{resp}}(t)dt, \quad (1)$$

which includes convolution with the intergrated system response function, $I_{\text{resp}}(t)$. (See the preceeding paper[2] for additional details). A nonlinear least-squares curve fitting routine[25] is used for the analysis of the experimental data to extract the state lifetimes and preexponential factors. Pulse widths may be determined from auto and cross correlations by using a variation of this routine.

III. SPECTROSCOPIC PHENOMENOLOGY

This section will acquaint the reader with the essential nomenclature for the HOOH and OH systems which will be used in the subsequent sections of this paper.

Preparation of a pure local-mode (LM) state requires that several rather exacting experimental factors be simultaneously attained. The bandwidth of the laser must be broad enough to span all of the molecular eigenstates which contribute to the formation of the local-mode coherent superposition state. The bandwidth should, however, not be so broad that additional states which do not contribute to the superposition state of interest are optically excited. The pulse duration must be sufficiently short to prepare the desired state and to be able to measure the subsequent dynamical evolution (dephasing). Our use of the work "local-mode" (LM) state is to indicate that the pump laser is tuned within the absorption band of the OH stretch, identified by the use of the Birge-Sponer relationship, as a local mode with a fundamental frequency of 3701 cm^{-1} and a diagonal anharmocicity of $-90.5\ \text{cm}^{-1}$.[6(a)]

The spectroscopy of HOOH at $v_{\text{OH}} = 5,6$, has been studied in Crim's group,[6(b)] and has built on the prelaser studies concerning the nature of the infrared absorption spectum of hydrogen peroxide.[9] Specifically, these developments include detailed modeling studies of the $v_{\text{OH}} = 5,6$ gas phase "predissociation" spectra,[6(b)] and have provided insight into the nature of the vibrational spectral features. Of particular interest to the work presented in this paper is the apparent success of adiabatically separating the OH stretch from the molecular torsional motion (in a manner analogous to the Born–Oppenheimer approximation), making possible the assignment of some of the more prominent spectral features. This has allowed the identification of three types of vibrational features (all of which have associated rotational structure) in the main fourth overtone absorption (i.e., predissociation) region, those due to: (1) pure overtone excitation; (2) hot band transitions involving the torsional motion; and (3) excitation features which include both O–O stretch (ν_3) and torsional hot bands. It should be reiterated that such high internal energy spectral features are prominent in the $v_{\text{OH}} = 5$ predissociation spectrum because the zero point of this transition is 1100 cm^{-1} below the D_0 value of HOOH. Hence, the transition features which presumably dominate the true absorption spectrum[26] are those which originate from appreciably populated ground state levels (Boltzmann distribution) and are not observed to be predominant in the fourth overtone predissociation spectrum.

The spectroscopy of the hydroxyl radical has been extensively studied[27] and is well understood, in contrast to the degree of knowledge of the overtone levels of HOOH. The dissociation products are formed in the two spin–orbit manifolds ($\Omega = \frac{1}{2}, \frac{3}{2}$) of the $X\,^2\Pi_\Omega^\Lambda$ electronic ground state and may undergo transitions to the two types of spin–rotation states (F_1 and F_2) of the $A\,^2\Sigma$ excited electronic state. The angular momentum quantum number N excludes the spin angular momentum ($S = \pm\frac{1}{2}$), and the total angular momentum is denoted by J, where $J = S + N$. Further characterization of these states is given by $\Lambda = (\pm)$, which describes orbital–rotation interactions. Because of the quasidegeneracy of the F states, the usual P, Q, and R transitions are further labeled according to the type of F levels (1 or 2) involved. The initial (in the $\Pi_{3/2}$ state) N quantum number is represented enclosed in the parentheses, e.g., $Q_1(1)$ for $N = 1$. For more details see the paper by Dieke and Crosswhite.[27] Since the spectral bandwidth of the probe laser is a few wave numbers in extent the e.g., $Q_1(1)$ and (the satellite branch) $Q_{21}(1)$ transitions are not distinguishable. This does not cause a problem in interpretation, however, because these transitions originate from the same Ω,N,Λ ground state level.

In performing polarization studies it is important to understand the degree of correlation between fragment angular momenta and the recoil velocity axis (this will not be detailed here). Time-integrated polarization experiments have been elegantly demonstrated on this and other related systems.[28] Only preliminary results of time-dependent polarization studies are presented herein. Relevant spectroscopic parameters of HOOH and OH are given in Table I.

IV. RESULTS

A. Fourth overtone predissociation studies

1. Pump wavelength and polarization dependences

Figure 4(a) shows an overtone pump OH product probe experimental transient for the $Q_1(1)$ transition (pump wavelength: 6142.5 Å). This transient was fit to a biexponential functional form, including a deconvolution for the response function; the resulting parameters are $\tau_1 = 80 \pm 10$ ps and $\tau_2 = 580 \pm 75$ ps with the value for the fraction, i.e., the ratio of the amplitude of the fast component to the total amplitude [see Eq. (1)], being 0.58. The transient in Fig. 4(b) is for a pump excitation wavelength of 6139 Å and the probe transition $Q_1(1)$, with fitted time constants of $\tau_1 = 54 \pm 7$ ps and $\tau_2 = 410 \pm 50$ ps, where $f = 0.37$. The notable features are that both transients exhibit quasibiexponential buildup behavior and that the values for the fraction differ considerably between these transients. The only essential difference in experimental conditions for the two measurements is the alteration of the pump wavelength. The variation in the fraction qualitatively follows the oscillations in the lifetimes—a smaller value for the fraction is seen in conjunction with longer time constants. It is interesting to note that a small change in the excitation energy results in dramatic changes in the transient behavior. This point will be analyzed in greater detail below and in the Discussion section. In general it has been found that each of the ob-

TABLE I. Spectroscopic constants used in calculations.[a]

Parameter	Value	Reference	Parameter	Value	Reference
		H_2O_2			
D_0(HO–OH)	49.6 kcal mol^{-1}	13	A''	10.063 cm^{-1}	6
D_0(HOO–H)	88.5 kcal mol^{-1}	44[b]	B''	0.8737 cm^{-1}	6
$r_{HOO-H,eq}$	0.965 Å	44	C''	0.8366 cm^{-1}	6
$r_{HO-OH,eq}$	1.462 Å	44	A'	8.74 cm^{-1}	6
ν_1	3599 cm^{-1}	44	B'	0.905 cm^{-1}	6
ν_2	1402 cm^{-1}	44	$h\bar{\nu}_0^0$	16250 cm^{-1}	6
ν_3	877 cm^{-1}	44	C_6	0.546 E6 cm^{-1} Å^6	
ν_4	c				
ν_5	3608 cm^{-1}	44			
ν_6	1266 cm^{-1}	44			
$V_{0,g}$	971.0 cm^{-1}	9	$V_{0,e}$	901.8 cm^{-1}	6
$V_{1,g}$	1093.4 cm^{-1}	9	$V_{1,e}$	903.5 cm^{-1}	6
$V_{2,g}$	546.7 cm^{-1}	9	$V_{2,e}$	835.6 cm^{-1}	6
$V_{3,g}$	− 56.4 cm^{-1}	9	$V_{3,e}$	84.0 cm^{-1}	6
$\chi_{0,eq}$	111.5°	6	$\chi_{5,eq}$	102°	6
$\alpha_{0,g}$	39.945 cm^{-1}	9	$\alpha_{0,e}$	35.0 cm^{-1}	6
$\alpha_{1,g}$	0.248 cm^{-1}	9	$\alpha_{1,e}$	0 cm^{-1}	6
$\alpha_{2,g}$	0.0433 cm^{-1}	9	$\alpha_{2,e}$	0 cm^{-1}	6
		OH			
ν	3735 cm^{-1}	44	$r_{OH,e}$	0.9710 Å	44

[a] The V_i are the torsional potential constants in the ground $V_{i,g}$ and excited $V_{i,e}$ states. $\chi_{i,eq}$ is the equilibrium torsional dihedral angle.
[b] See Ref. 44 for the original references of the listed parameters.
[c] These values are determined from the potential parameters, see the text and Appendix.

served transients corresponding to the $N = 1,2$ OH transitions may be modeled as a rising biexponential buildup of the OH photoproduct. All of the results to be reported are for parallel pump–probe polarizations, unless otherwise specifically indicated.

A more detailed analysis is presented in Fig. 5(a) which shows an expanded scan of the initial component of the 6142.5 Å pump $Q_1(1)$ probe transition. The system response function is also displayed to indicate the substantial difference between the fast buildup and the response. Both the transient and the cross correlation correspond to exactly the same scan range. The $t = 0$ of the response function is seen to occur substantially earlier than the half-maximal value of the transient signal level. This clearly illustrates that the fast component has a substantially longer lifetime than the duration of the system response. The response displayed in the figure is used in fitting the experimental transient. The fitted exponential lifetime for this initial portion of the quasibiexponential buildup [seen in Fig. 5(a)] is 75 ± 5 ps. This is in good agreement with the lifetime obtained from the long delay-time scans. The response function is determined to have a Gaussian functional form with, approximately, a 10 ps FWHM. The shape is actually slightly asymmetric reflecting the asymmetry of the oscillator pulse(s).

In addition to the greater portion of the data being for parallel pump–probe polarizations, several transients with perpendicular polarizations were obtained. Performing these ∥ and ⊥ polarization studies with the same experimental conditions yields a result *on the transients* (not yield) since identical parameter values, within the fitting errors, are obtained. Since the effective B constant ($\frac{B+C}{2}$) is about 0.86 cm^{-1} and $\langle J \rangle \approx 23$ for the molecules with sufficient energy to undergo dissociation, the period for the rotational motion associated with the largest moment of inertia is on the order of a picosecond or less. This is substantially faster than the most rapid observed rate of dissociation. Experiments using proper geometry for anisotropy detection[28] are in progress.

The effects of variations of the specific pump excitation wavelength on the $N = 1$ transient behavior are compiled in Table II. The different pump excitation energies ($h\nu_{pump}$) cause the prompt components of the biexponential rises to change in duration in a *nonmonotonic* fashion. The long components change in a similar manner but not necessarily by a uniformly proportional amount, the only exception to this trend being the transient associated with the $P_1(1)$ transition. It may be noticed that there is a strong correlation for the two lifetime components in that they become longer or shorter together. The table also lists the fraction. There is a correlation of the value of the fraction with the trends seen for the lifetimes; the smallest value for the fraction occurs in conjunction with the shorter time constants. The pump-energy selective dissociation rates as well as a predissociation spectrum adapted from Ref. 6 is shown in Fig. 6. This figure makes manifest the close correlation between the two time constants and the fraction at each excitation wavelength. It is not as straightforward to associate specific spectral features with the observed lifetimes. This issue of the transient dependence on the pump wavelength will be addressed more completely in the discussion section by comparing the ob-

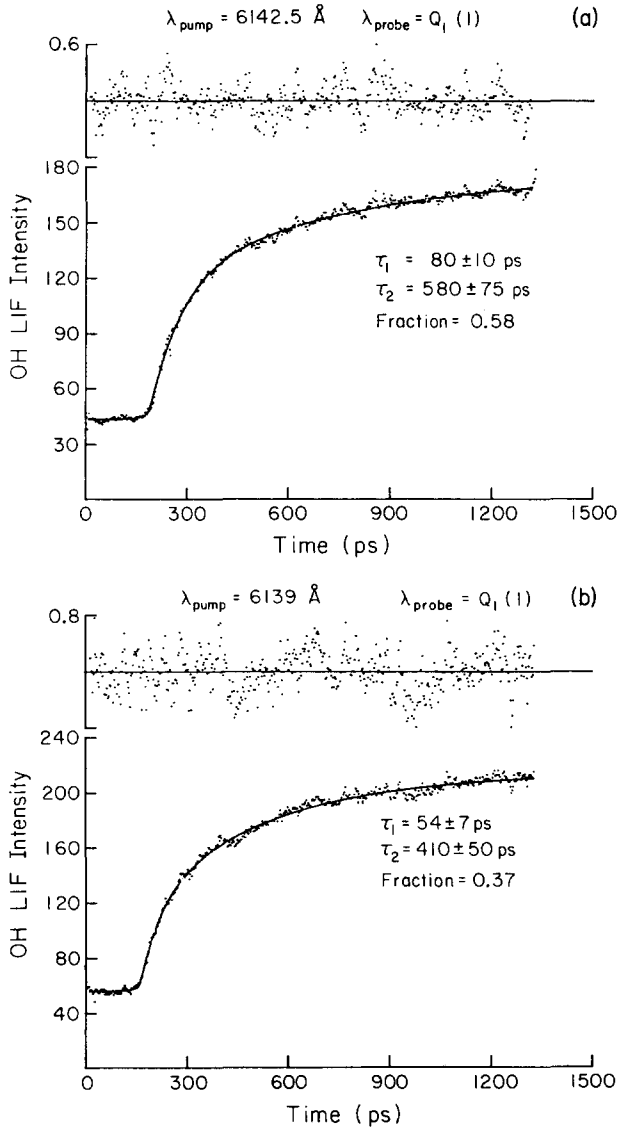

FIG. 4. Experimental results showing the ubiquitous biexponential behavior. The lifetimes and the fraction are indicated, the experimentally changed condition [between (a) and (b)] is the excitation wavelength. The residual for each transient shows the adequacy of a biexponential model function to simulate the behavior. Other transients, similar in form to those shown here, were obtained—the fitting parameters are given in Table II.

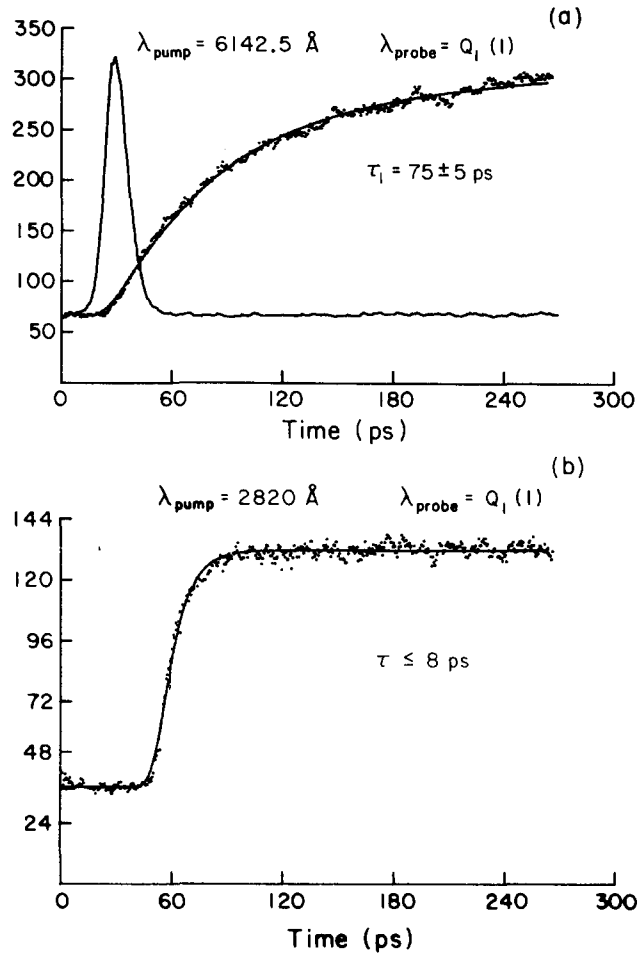

FIG. 5. Short component and the response function, (a). This corresponds to the fast component in Fig. 4(b). The response function is seen to be noticably shorter than the rise. A single exponential fit, using the same response is the fitted curve through the data. The UV–UV transient and the fitted single exponential are shown in (b). There is no biexponential behavior discernable in (b).

served behavior with the results of statistical rate/spectral model studies.

2. Probing different OH states

The results for the $N = 2$ Q-branch transitions show markedly different behavior than the $N = 1$ transitions for the same pump laser excitation wavelength. The short and the long lifetimes are somewhat different than the corresponding $N = 1$ results, the long time constant having changed by a more significant amount. The most dramatic difference is found in the change in the value of the fraction from about 0.4 to more than 0.7 in both cases (the precision of the individual results is about $\pm$ 0.05). The experimental result is shown in Fig. 7. The difference between this $N = 2$ result and the results shown in Fig. 4 are quite clear—the value for the fraction has changed significantly. The differ-

TABLE II. Dependence of experimental transient on excitation wavelength.

Probe transition	Pump λ ($\pm$ 0.5 Å)	τ_1 (ps)[a]	τ_2 (ps)	Fraction
$Q_1(1)$	6011 Å	51(8)	515(75)	0.53
	6029 Å	45(7)	310(50)	0.35
	6038 Å	32(5)	240(40)	0.32
	6098 Å	35(5)	300(50)	0.41
	6129 Å	40(5)	300(50)	0.40
	6132 Å	83(10)	610(100)	0.61
	6139 Å	54(7)	410(50)	0.37
	6142.5 Å	80(10)	580(75)	0.58
	6144 Å	91(10)	600(100)	0.63
	6146 Å	80(10)	570(75)	0.63
	6149 Å	65(8)	430(50)	0.60
	6157 Å	60(7)	580(75)	0.58
	6160 Å	52(8)	510(75)	0.43
$R_1(1)$	6136 Å	50(8)	540(75)	0.30
	6144 Å	95(10)	650(100)	0.57
	6157 Å	50(8)	550(75)	0.59
$P_1(1)$	6163 Å	45(8)	700(100)	0.65
$Q_1(2)$	6140 Å	43(8)	350(50)	0.72
	6160 Å	50(8)	400(400)	0.72

[a] The error bars represent $\pm$ 1 standard deviation for the fitting parameters.

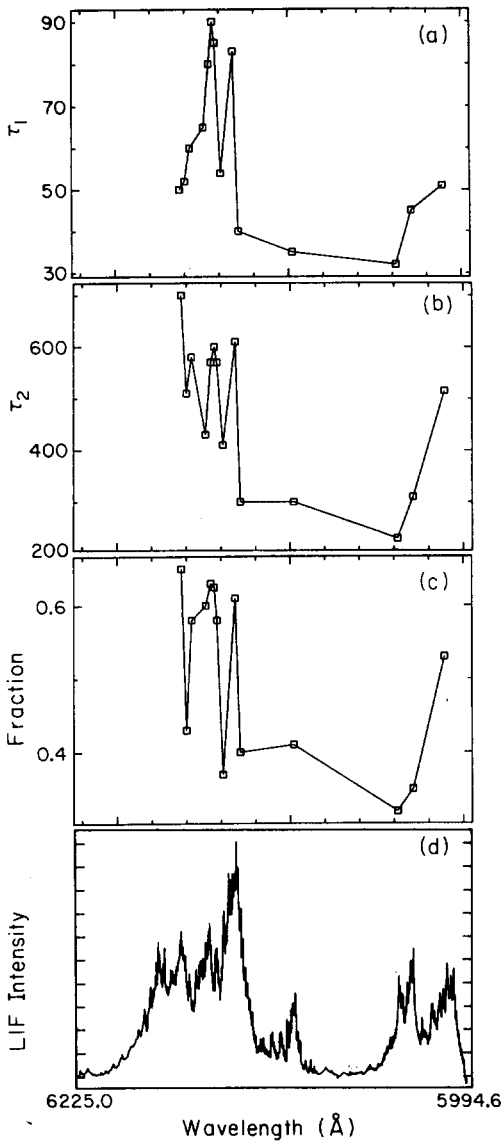

FIG. 6. The pump excitation wavelength dependent fluctuations in the short (a), and long (b), lifetimes (τ is in units of picoseconds) and the fraction (c). The predissociation spectrum [detecting $Q_1(1)$] of (d) is adapted from Ref. 6. The wavelength axes are all to the same scale. The fluctuations in the parameter values (also listed in Table II) may be examined for correlations.

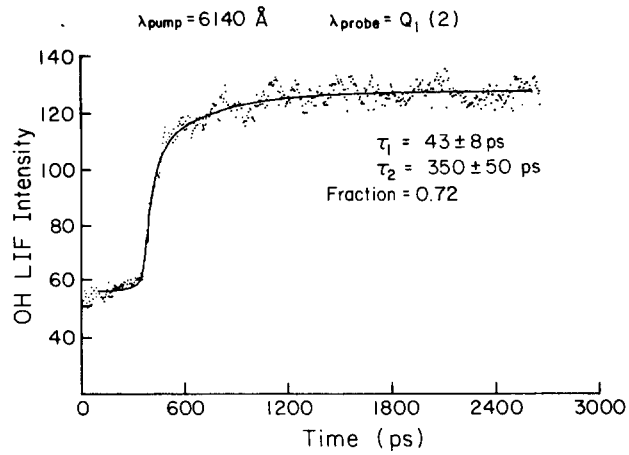

FIG. 7. Transient for $N = 2$. Probe is interrogating $Q_1(2)$. A biexponential fit gives the listed parameters. The time axis is twice that of Fig. 4(a). The excitation wavlengths for Fig. 4(a) and the present figure are the same ($\pm$ 1 Å). Only the probe transition is changed such that the OH fragment interrogated contains one quantum more rotational energy.

ence between the $Q_1(1)$ and the $Q_1(2)$ may be qualitatively understood in that some of those states closest to the barrier which form the $N = 1$ product may not be sufficiently energetic to form the $N = 2$ product.

In comparing the observed parameter of the Q-branch probe transitions with those for the R-branch transitions for the same pump wavelength, it is found that they are essentially equivalent, for the precision of the measurements. Within the limits of sensitivity of these experiments and for $N = 1$ there does not appear to be a Λ quantum number dependence for the time constants or fractions.

B. Diagnostic studies

1. Collison-free conditions

Several different control or diagnostic experiments must be performed to aid in the interpretation of the primary studies. Assurance that the results are collision-free for the duration of experimental interest (3 ns) is presented in Fig. 8(a). This figure shows a decay curve, for the $R_1(1)$ OH product transition (pump wavelenth: 6157 Å, pressure: 300 mTorr), which is the lifetime of the OH in the excited $A\ ^2\Sigma$ state. The transient, with a single exponential time constant of 424 ns, is shorter than the collision-free lifetime observed by others ($\tau \approx 800$ ns).[29] The collision period estimated from the hard sphere collisions is on the time scale of several nanoseconds (see Refs. 23 and 24 and references. cited therein). It has been previously observed that (ground state) rotational equilibration also takes place on a several hundred nanosecond time scale.[6(a)] The early-time deviation from a single exponential decay indicates the degree of over counting of the early bins, which may occur in single photon counting detection schemes. The TAC can process at most one event per laser shot. The pulse height distribution becomes skewed to early time when the event rate becomes too large. Since the OH lifetime signal was accumulated at the maximum pump–probe time delay, and hence maximum signal level, the small amount of over counting seen ($< 5\%$ of the total intergrated signal) has no significantly measurable (for the observed S/N) saturation effect on the transient. In general, the Baratron was used to monitor the cell pressure, which was maintained at $\leqslant$250 mTorr, ensuring a collision-free environment for all measurements. The decay of Fig. 8(a) is therefore a worst case condition in terms of mean time between collisions. The time scale being considered here is much longer than the pump–probe picosecond delay time scale.

2. Power dependence and two-photon processes

The power dependence of the OH LIF signal on the pump field intensity has been determined and Fig. 8(b) shows that the behavior is linear (the slope is equal to one within the experimental error). This is consistent with the picture that the fourth overtone is actually being interogat-

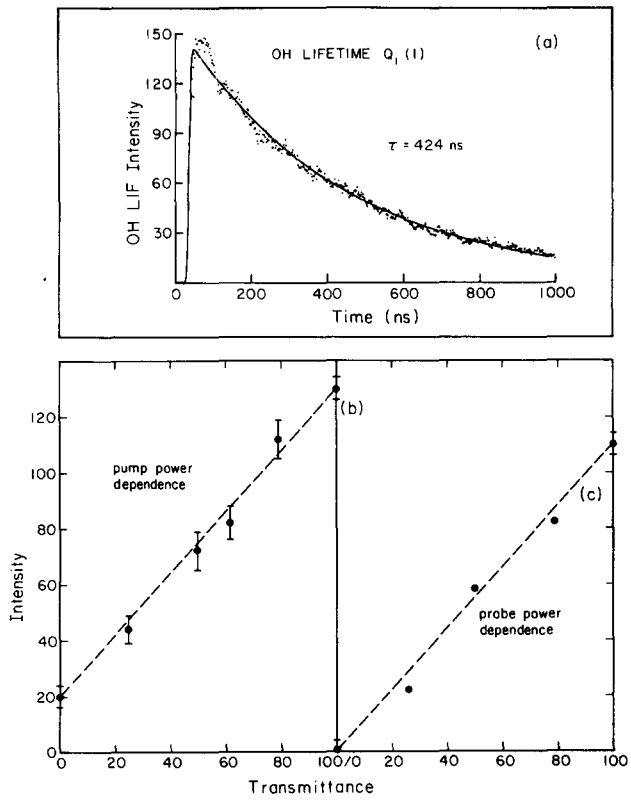

FIG. 8. Diagnostics. Top (a), shows the OH excited state lifetime. The transient was obtained at the maximum pump–probe delay setting and for a cell pressure of 300 mTorr. This decay is obtained by using the TAC in pulse-height analysis mode. The visible (pump) and UV (probe) power dependences are shown in (b) and (c), respectively. The linear trends are indicated by the dashed lines.

ed, and that the dynamics are not representative of some pumping scheme (e.g., two-photon to dissociation) which causes dissociation via a repulsive higher lying potential energy surfaces(s) of HOOH.[6,10] If the pump pulses are blocked, a steady state background (usually $\leqslant$25% of the total signal) remains. The background signal is reflected in the non-zero intercept in Fig. 8(b). This signal stems from the probe pulse interogation of a dissociative electronic state of HOOH and the same pulse probing the OH products formed.

A power dependence study of the probe field is performed to determine whether the behavior is consistent with the proposed mechanism of Fig. 1. The results of the UV beam intensity dependence study are presented in Fig. 8(c). The UV alone signal is subtracted from the total signal level at each point. This signal is time independent since it depends only on the presence of the probe pulse, and it does not contribute to the observed transient behavior. Furthermore, the pump–probe signal cannot be due to wall decomposition of HOOH since this would also result in a time independent signal. Blocking the probe beam shows that there is no observable signal from the pump field alone. The presence of this pump field only effect was examined at all of the different pump wavelengths used—such a two-photon signal has not been observed.

Verification that the LIF signal is due to OH is established by tuning the probe laser off-resonance of a specific $^2\Sigma \leftarrow {}^2\Pi$ OH transition and observing the signal disappear. Closing off the Teflon needle valve, which then isolates the HOOH reservior from the fluorescence viewing region of the cell, and evacuating the cell eliminates the LIF signal. The power dependence and other diagnostics show that the observed signal is consistent with the scheme of pump excitation of HOOH ($v_{OH} = 5$) and subsequent probe beam interrogation of the OH photodissociation product. This is further confirmed by the results of Sec. IV A 3. below.

3. Excited electronic state interrogation

The transient behavior which results from direct excitation of a dissociative electronic state of HOOH is useful for the interpretation of the constituent nature of the two components of the biexponential transient buildup. An alternative experimental arrangement is required for this study.[30] Since UV light of $\lambda \leqslant 300$ nm is required to make the transition with a reasonable absorption cross section[7] (in order to obtain a useful degree of enhancement), a Raman shifting method (involving CH_4) is employed to generate anti-Stokes shifted ($+2914\ cm^{-1}$) light of the fundamental frequency of DL1. The mixed light (anti-Stokes shifted plus fundamental) of 282 nm is generated as the new pump field, while the probe frequency is maintained in resonance with the $Q_1(1)$ OH transition. Figure 5(b) shows the resultant transient to be a single exponential rise which has a time constant of less than 8 ps—there is no long component present. Even though the pump wavelength is somewhat different than twice the frequency of the visible overtone pump field, it is seen that the transient shape and the single lifetime component differs substantially from those of Fig. 4. For the sake of making a clear distinction of the difference in the transient behavior due to visible or UV proton dissociation of HOOH, it may be recalled that Fig. 5(a) is an expanded view of the initial buildup of 6142.5 Å pump $Q_1(1)$ probe transient. The abscissa of the UV pump transient has the same scale calibration as Fig. 5(a) but the time-zero is different for the two plots. It is clear that the prompt reaction rates for overtone predissociation and direct dissociation are extremely different, especially when taking into account the fact that the response functions only differ by about 25% [see the rise of the signal in Fig. 5(b)].

It has been previously mentioned (Experimental section) that the response function for the UV-pump–UV-probe transient is not directly obtainable. A deconvolution of this transient with a (simulated) 9 ps Gaussian response yields, unlike all of the visible pump transients, a single exponential buildup with a lifetime of the same order as the response duration, that is $\tau \leqslant 8$ ps. This number is an upper-bound, and is consistent with earlier work[10,28] which deduces the lifetime from alignment experiments for excitations of 248 or 266 nm. Further studies, similar to those reported in Ref. 31 (femtosecond photofragment spectroscopy), are in progress to give more precise measurements for the HOOH excited electronic state lifetimes into specific Λ,N,Ω product states. The main conclusion to be reached from this study is that the time-dependent behavior of the

excited electronic state is quite different from that observed for direct overtone pumping and that this (along with the power dependences) is conclusive in showing that the (visible excitation) transients are not due to some sort of multiphoton effect of the pump field.

V. DISCUSSION

The preceding exposition of the overtone pump experimental results indicate three important observations. First, the product buildup rates are quasibiexponential. Second, these same rates (and the fraction) behave nonmonotonically with respect to changes in the pump wavelength. Third, the contribution of the dissociation time constants(s) to the linewidth (only 0.05–0.15 cm^{-1}) is several orders of magnitude less than the apparent width. This section will be devoted to gaining further insight into the significance of these observations and the dynamics which they reflect. The aim will be to determine the degree of applicability of statistical and nonstatistical theories in explanation of the results. The first part of the discussion will be concerned with the source of the biexponential transient behavior. The second portion of this section will be devoted to understanding the unique energy dependence of the transients. In the final part of the discussion, some remarks are made comparing the results of linewidth studies to the real-time measurements of IVR and reaction rate.

A. Quasibiexponential behavior

To begin the discussion suppose, for the moment, that the lack of available spectral information is such that spectral transition frequencies and states cannot be assigned. If the intramolecular dynamical behavior is considered to be statistical then the expected unimolecular reaction behavior is expected to conform to a single exponential decay rate. Conventionally, the averaged rate constant is related to the microcanonical rate constants $k(E_x)$ by the expression[32]

$$\langle k(T,E_x)\rangle = \frac{1}{Q}\int_0^\infty k(E+E_x)\,\rho(E)\cdot e^{(-E/k_BT)}dE, \quad (2)$$

where Q is the vibrational partition function, E refers to a given thermal energy, E_x is the excess vibrational energy, and $\rho(E)$ is the state density. In general, $k(E_x)$ may be evaluated using the RRKM expression or some variation thereof. In the simplest form $k(E_x) = A\,[\exp(-B/E_x)]$, where A and B are constants. The resultant rate of product formation is embodied in the single (average) exponential rate constant.

Two causes for the deviation of the experimental results from such single exponential behavior may now be realized. Firstly, the probability of mode occupation following the overtone excitation is no longer related to the internal temperature by a Boltzmann distribution. Secondly, the nonexponential behavior may stem from a division of the rovibrational phase space of the molecule.[32,33] The division creates two (or more) classes of initial states which are distinguishable by their associated reaction rate behavior. Our observation of biexponential behavior could, therefore, be related to nonstatistical behavior provided one exludes the effects of proper thermal averaging and thermal state distributions. In what follows, such effects will be carefully examined to elucidate the implications for the resultant behavior.

1. Thermally averaged rate

To begin, consider the microcanonical rate constant (k_{MC}) to be that which is defined by the well known RRKM expression

$$k_{MC}(EJ) = \frac{N^{\ddagger}_{E^*J}}{h\rho_{EJ}}, \quad (3)$$

where $N^{\ddagger}_{E^*J}$ is the state count in the critical configuration for the given model of the reaction with energy $E^* = E - E_0$ (for $J=0$) above the critical energy for reaction, ρ_{EJ} is the state density in the reactant. The probability at time t of having formed a specific product from molecules excited to the fourth overtone level is obtained by averaging the microcanonical RRKM rates of reaction over the internal energy distribution, and may be expressed by

$$P_N(t) = \sum_{J=0}^{\infty}\int_o^\infty p_N(EJ)\cdot p^0_{EJ}\cdot\{1-e^{[-k_{MC}(EJ)\cdot t]}\}dE, \quad (4)$$

which is then evaluated as a function of time to obtain the transient waveform. The original energy and J distributions, the associated Boltzmann distribution and state density are contained in p^0_{EJ}, while $p_N(EJ)$ is the probability that the system is in any of the final quantum states (product state distributions).

In performing the calculations for HOOH, the values for the microcanonical rate constants, $k_{MC}(EJ)$, were determined by combining the value for the number of states in the critical configuration ($N^{\ddagger}$) for a loose transition state, phase space theory (PST), calculation with the density of reactant states obtained from a direct state-count routine. The reader is referred to Table I for some details of the parameters used in the calculations (see Sec. V B below and the preceeding paper[2] for a discussion of PST).

Figure 9 displays the simulated transients [plot of Eq. (4) vs time] for the $N=1$ and $N=2$ OH product rotational levels as curves 1 and 4, respectively. The calculated behavior, as seen in curve 1, is qualitatively similar to the observed experimental behavior in that the calculated transient is nonexponential (quasibiexponential) in nature. Notice the rapid buildup behavior of $N=2$ as compared to $N=1$. The fitted lifetimes and fraction, as presented in Table III, show the same relative trends as the experimental $Q_1(1)$ and $Q_2(2)$ results. The fast and slow component lifetimes for the $N=2$ transient are shorter than for $N=1$ and the contribution of the fast component to the total amplitude becomes larger (i.e., the fraction increases). The calculation was performed for laser excitation energy of 16 255 cm^{-1} which is equivalent to the 0–0 transition frequency determined from a Birge–Sponer plot.[6] The barrier to dissociation is 1100 cm^{-1} above this value, so only molecules in the tail of the thermal distribution are potentially reactive. The OH product state distribution, which is obtained as a by-product of this calculation, is typically peaked at $N=1$ and is (generally) a monotonically decreasing function of N. The experimentally measured product state distribution[6] is peaked at $N=1$ and

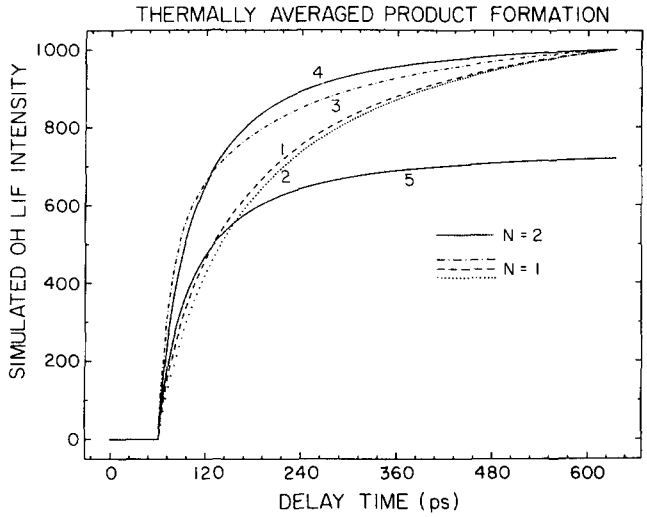

FIG. 9. Phase space theory (thermally averaged) calculation of product state probability vs time. Curve 1: $N = 1$, curve 2: $N = 1$ "cold" distribution, curve 3: $N = 1$ "hot" distribution, curve 4: $N = 2$. All four curves are normalized to the same final value to enhance the effect of different parameters on the calculated signal. Curve 5: $N = 2$ intensity, relative to $N = 1$. The time scale for all of the transients is half that of Fig. 4. This is done to aid the distinction of the curves near the breaks for the two components of the quasibiexponential behavior. The results of the biexponential model fitting are given in Table III.

P_N is also monotonically decreasing with increasing N. It is interesting that the thermal average of the microcanonical rates and distributions give qualitative trends which agree with the experimentally measured rates and product state distributions.

2. Nonstatistical perspective

It was suggested in our earlier communication[5] that a divided vibrational phase space may also account for the observed quasibiexponential product buildup dynamics. This is similar to the resultant behavior of a model advanced for IVR by Perry *et al.*[32] Marcus and Hase have recently indicated that nonexponential behavior could be explained if the phase space of the molecule were divided in a way representative of the directness with which a (classical) trajectory crosses the transition state to dissociation.[33] The *a priori* assumption is that the phase space of the system is noncommunicating on some portion of the time scale of the measurement, such that this non-RRKM behavior becomes manifest.

A two part divided phase space model yields a biexponential decay of reactant systems. For illustration, assume the following scheme (see Refs. 32, 33, and 39 for development of the model for the description of IVR and reactions):

$$N_2 \underset{k_2}{\overset{k_3}{\rightleftharpoons}} N_1 \overset{k_1}{\rightarrow} \text{products},$$

where N_1 and N_2 are the populations of the two subspaces. For the experimental results presented herein the implication of the observed biexponential product (OH) buildup is that the slow component is described by the RRKM rate while the fast component is determined by $k_2 + k_3$. A necessary conditon is that $(k_2 + k_3) \gg k_1$ and that the slower (RRKM) component is much different than the fast one, as discussed by Marcus.[33] This non-RRKM behavior is physically intuitive: at short times the phase space is divided and only the trajectories initiated in one portion thereof may cross the transition state, while at long times the system equilibrates and reaches the statistical limit behavior. The long time component observed in the present experiments falls in the range of 300 to 700 ps. In comparison, the fast component is 40–90 ps. It is therefore tempting to ascribe the biexponential transient behavior to nonstatistical effects, where the RRKM rates at these energies should be given by the values for the slow rise. Standard statistical calculations performed near the threshold yield values for the RRKM time constant close to the 300–700 ps range expected. Furthermore, at all energies of excitation the transient behavior is still biexponential and only the values of the rate constants change. One's exuberance must be restrained, however, because of the other possible explanations discussed herein.

In paper III,[34] the model of a divided phase space is used to account for the biexponential decay observed in the photodissociation of beam-cooled van der Waals molecules (this is interpreted as non-RRKM behavior). For that case the initial distribution (p^0_{EJ}) is very narrow (beam experiment). The thermal conditions of the present study, however, make the analysis more difficult. To fully examine the specifics of such non-RRKM behavior it is desirable to rigorously specify the initially prepared state and the internal energy. This last point constitutes the efforts of work in progress.

Recently reported classical trajectory studies[12] of the intramolecular and dissociation dynamics of hydrogen peroxide excited to the fifth overtone level—one quantum higher than the present study—show evidence for incomplete (vibrational) energy redistribution on the time scale of reaction. This is quite interesting and lends support to the aforementioned divided phase space model. These calculations showed that most of the vibrations are strongly coupled (on the time scale of the reaction). The exception being the OH oscillator which is initially unexcited. The exact nature of the division of the phase space must await more complete calculations which include rotation–vibration coupling and which are performed using a more refined (perhaps *ab initio*) potential energy surface. It would be interesting to perform these calculations for energies near the threshold. For comparison with theory experimental investigations for $v_{OH} = 6$ are in progress.

The next salient point to be understood is whether the nonmonotonic behavior of the rates with excess energy may be used to test for nonstatistical effects. An alternative issue is the effectiveness of statistical calculations (using the known spectral information) in simulating the same effects. These points shall be addressed in the following section.

TABLE III. Thermal averaged calculations.

Curve no.	Parameter	Energy (cm^{-1})	τ_1 (ps)	τ_2 (ps)	Fraction
1	($N = 1$)	16 250	46	270	0.36
2	cold	16 250	68	300	0.42
3	hot	16 250	23	225	0.48
4,5	($N = 2$)	16 250	38	215	0.59

B. Dependence of rates on photon energy

Coming to an understanding of fluctuations in the values of the reaction rates and fraction as a function of excitation energy is perhaps the more interesting of the two main issues which this Discussion section is intended to address. This is because the nonmonotonic behavior may reflect nonstatistical behavior. However, caution must be exercised since several explanations of the observed behavior are possible. These various interpretations will be investigated and the domain of their applicability examined, after discussing the effect of (conventional) thermal averaging.

1. Thermally averaged rates

To begin, assume that no transition frequency information is available. This implies transfering the ground state thermal distribution to the level of the fourth overtone. Consider the behavior which may be observed: (i) Sec. V A established that a quasibiexponential buildup behavior is to be expected; (ii) tuning the laser to greater energy (shorter wavelength) would have the effect of making the excited molecule acquire more internal energy, therefore, the expectation is for the reaction rates to increase monotonically with laser excitation energy. Intuitively, the state count in the transition state increases more rapidly than the state density (ρ_{EJ} changes by a factor of 3 over 2500 cm^{-1} beginning at 16 250 cm^{-1}) in the reactant for a given δE increase in the excitation energy. Therefore, the rate expression of Eq. (3) would be overall increasing with excitation energy. The expectation is for the rates to change monotonically with laser energy.

From the data for the initial component lifetime from Figs. 4 and 6 and Table II it may be seen that the behavior is hardly monotonic. Without invoking any further spectral knowledge concerning the fourth overtone it might be concluded that the behavior is nonstatistical. This conclusion, however, ignores the reality that excitation of different portions of an inhomogeneously broadened overtone band prepares different (in this case) initial distributions of states. The specifics of the excitation have a direct bearing on the subsequent unimolecular dynamics. Again, this nonstatistical mode-specific rate behavior may only be unequivocally demonstrated when the optical preparation is of a single (homogeneously broadened) spectroscopic state.

2. Effect of nonuniform state distribution

Now consider the resultant transient behavior, in the spirit of Eq. (4), for the case where the specific transition frequencies are still not known but the distribution of states excited to the fourth overtone level is non-Boltzmann. The idea is to examine the effect of enhancing (or diminishing) some portion of the tail of the probability distribution by generating the corresponding transient. In the thermally averaged calculation, the average J of reacting molecules is $\langle J \rangle = 23$ while the average reactant state energy above the 0–0 transition energy $\langle E \rangle \approx 1700\ cm^{-1}$ (recall that the barrier height with respect to this same reference is 1100 cm^{-1}). To simulate the effects of "hot" and "cold" nonthermal distributions, the (Boltzmann) distribution factor $\exp(-E/k_BT)$ was changed to $\exp^{[(\alpha - E)/k_BT]}$ with

$$\alpha = \begin{cases} 0, & E \leqslant 1600 \\ 500, & E > 1600 \end{cases} \text{ and } \begin{cases} 0, & E \leqslant 1600 \\ -650, & E > 1600 \end{cases}$$

for the hot and cold distributions, respectively. The values for α are expressed in units of cm^{-1}. The results are depicted in curves 2 and 3 of Fig. 9, and the fitted values are in Table III. Notice that by adjusting only the probability distribution the resultant transients (lifetimes as well as the fraction) are affected. One conclusion is that the specific variations in the distribution of optically prepared states may be the underlying cause of the experimentally observed fluctuations.

As a further illustration of the physical picture consider the model four level system—two ground states (1′ and 2′) optically coupled to two excited states. The latter two states (1 and 2) are sufficiently energetic to undergo reaction with rate constants k_1 and k_2. The corresponding absorption coefficients are ϵ_1 and ϵ_2. If the reaction proceeds exclusively to products in state m then a biexponential product buildup is observed with the aforementioned rates and fraction $\epsilon_1/(\epsilon_1 + \epsilon_2)$. Now cosider that the two excited levels of this four level system become two sets of levels with reaction rates $\{k_i\}_1$ and $\{k_j\}_2$ for reaction into the exclusive product quantum state m. Each absorption coefficient now refers to the respective set of levels. If there is no intersection of the two sets, and the members of each set are distributed such that the rates of one set are faster than the other, but within a set there is a distribution of rates, then preparation of one set or the other will result in a distribution of rates in the product buildup behavior. If both sets of states are prepared and if the difference in rates between the two sets is larger than the extent of the distributions within the sets, then a quasibiexponential transient behavior will be observed. The fraction will be essentially the same as before.

3. Effect of rotations

Variation of the J value for a given reactant energy can have a pronounced effect on the reaction rate especially near threshold. This is predicted by other statistical theories[35] as well. The conserved quantum numbers restrict the domain of the phase space (for the given E and J). The restriction imposed by J affects $N^{\ddagger}_{E^*J}$ and ρ_{EJ} differently, therefore, the rate varies with J. The implication is that this variation may have a strong influence on the observed rates of reaction because the average value of J may differ for various portions of the action spectrum for the fourth overtone. This point will be investigated more carefully in the following section.

4. Effect of combined spectral and thermal distributions

The focus of this section is to attempt to simulate the experimental biexponential and nonmonotonic behavior of the rates. This will be done by explicitly considering the spectral and E,J distributions of the initial excitation to the fourth overtone. Crim and co-workers[6(b)] have considered the spectral consequences of making an adiabatic separation, in the spirit of the Born–Oppenheimer approximation, of the rapid OH stretching motion from the low frequency torsional motion about the O–O bond. Implementation of this

method has allowed them to empirically fit the major features of the predissociation spectrum to: (i) hot band transitions of the torsional and/or O–O stretching mode; (ii) sequence band transitions; and (iii) combination bands of torsion with the $\Delta v_{OH} = 5$ overtone transition. It should be reiterated that these features would seem to be dominant in the predissociation spectrum since a zero-point transition to $v_{OH} = 5$ (as determined from the HOOH Birge–Sponer plot[6]) leaves the peroxide molecule 1100 cm^{-1} below the barrier to dissociation.

Using their recently reported torsional potential parameters[6(b)] and the analogous parameters for the ground state,[9] we have evaluated the transition frequencies from the initial and final eigenvalues (relevant to the $\Delta v_{OH} = 5$ transition), which were calculated as the solutions of a tridiagonal matrix of difference equations. The eigenvectors then were obtained using the same numerical routine and applied in the determination of the associated transition intensities. The time integrated intensity of product formation into a specific OH product state $N(\Omega = \frac{3}{2})$ is given by

$$I(E,J,K;N) = C\bar{\nu}A_{KJ}P'^{0}_{EJ}P_N|\langle v'\tau'|\hat{\mu}|v''\tau''\rangle|^2, \qquad (5)$$

where C is a constant ($\frac{8\pi^3}{3hc}$), $\bar{\nu}$ is the transition frequency in cm^{-1} units and τ is the torsional quantum number. The Boltzmann weighting factor for energy E and degeneracy terms are included in P'^{0}_{EJ}, P_N is the probability for formation of the OH product in state N, and A_{KJ} are the Hönl–London factors for (as an approximation[6]) $\perp$ prolate symmetric top transitions.

Since the OH stretching and torsional motions are assumed to be separable, the transition moment may be decomposed into those portions with projections onto the stretch and torsional coordinates. The term for the square modulus can therefore be rewritten as $|\langle v'|\hat{\mu}|v''\rangle\langle\tau'|\tau''\rangle|^2$. This is in accord with the assumption of the OH overtone behaving as a LM state—that is $\hat{\mu}_{torsion} \sim 0$. It may now be seen that the intensity of hot band or combination transitions are dictated by the torsional mode overlap integral. The eigenvalues and therefore the transition frequencies indicate that there are three types of features in the fourth overtone band: (i) the spectral feature near 16 200 cm^{-1} (6173 Å) is enhanced by contributions from ν_3 (O–O stretch) hot band transitions; (ii) the region near 16 240 cm^{-1} (6158 Å) is enhanced by the presence of torsional hot band transitions; while (iii) the feature near 16 300 cm^{-1} (6134 Å) is most prominent because this is the region with the highest density of allowed transitions which have sufficient energy for dissociation. This is elaborated more explicitly by the values of $\langle J \rangle$ and $\langle E_{vib} \rangle$ listed in Table IV. The values for $\langle E_{total} \rangle$ as a function of laser excitation wavelength, which are not listed, fall in the range 1700 ± 100 cm^{-1} above the lowest rovibrational level of the fourth overtone.

A classical phase space theory is invoked in the calculation of the rates and product state distributions (PSD), and is combined with the above described spectral analysis. PST gives P_N for a given E and J. (The value of the C_6 parameter is 0.546×10^6 cm^{-1} Å^6.)[36] P_N is evaluated for each specific transition allowed within the simulated laser bandwidth. The relative intensities of the formation of product into the

TABLE IV. Calculated transient parameters including all spectroscopic transitions.

Probe trans.	Pump λ	τ_1 (ps)	τ_2 (ps)	Fract.	$\langle J \rangle$	$\langle E_{vib} \rangle$	No. trans.
$N=1$	6129	45	280	0.51	18.8	1040	185
	6132	60	270	0.22	17.6	1130	190
	6139	55	280	0.30	15.5	1310	180
	6142.5	100	315	0.43	15.5	1420	165
	6144	75	330	0.49	16.5	1455	150
	6146	85	300	0.57	17.0	1525	135
	6149	50	280	0.29	16.4	1620	120
	6157	45	290	0.39	16.3	1610	105
	6160	45	250	0.46	15.5	1630	110
	6163	30	350	0.87	16.2	1655	95

$N = 1$, 2, and 3 states as a function of excitation wavelength is obtained by summing Eq. (5) over all possible transitions and weighting each optical transition by the simulated laser bandwidth. This calculation allows for making a coarse-spectral-resolution comparison with the action (or predissociation) spectrum measured in Ref. 6. The agreement is good enough to be able to discern the major features observed in the experimental spectra for $N = 1$, 2, and 3. These results, which are highlighted in Table IV for different excitation energies, will be presented in more detail in another publication[37] (also see the Appendix). It suffices to say that the spectral simulation is faithful to the actual results and enhances the reliability of the simulated transients obtained below.

The time-dependent intensity of product formation into state N can be expressed, in analogy with Eq. (4), in a manner representative of the individual optically allowed transitions. Indexing these transitions by i and combining Eqs. (4) and (5) gives

$$P(N,t) = \bar{\nu}\sum_i M^i(A^i_{KJ})L(\delta,\bar{\nu})P^i_N \cdot P'^{0i}_{EJ}\cdot\{1 - e^{[-k_i(EJ)\cdot t]}\}, \qquad (6)$$

where $M^i = C|\langle v'|\hat{\mu}|v''\rangle|^2|\langle\tau'|\tau''\rangle_i|^2$, the laser bandwidth functional form $L(\delta,\bar{\nu})$ is Gaussian, FWHM: 3.0 cm^{-1}, P'^{0i}_{EJ} is the Boltzmann factor for the given E and J of the ith transition and $k_i(EJ)$ is the microcanonical rate for the ith transiton. For a simulated laser bandwidth of 3.0 cm^{-1} there are typically more than 100 possible optical transitions.

The form of the simulated transients are quasibiexponential rises (as opposed to single exponential), albeit there is a large diversity in the calculated behavior for the variously chosen transition energies $\bar{\nu}$ as listed in Table IV (see Fig. 10). There is some correlation between the experimentally measured fast component (Table II) and the transient value calculated here.[38] The correlation is achieved essentially independent of adjustable parameters, (i.e., there has been no fine tuning of the results) within the limits of the assumptions invoked in applying PST, in obtaining the density of states, and in only considering optical transitions involving the torsional and O–O stretching modes in determining the discrete transitions. The calculated long component lifetimes are about a factor of 2 to 3 faster than the measured

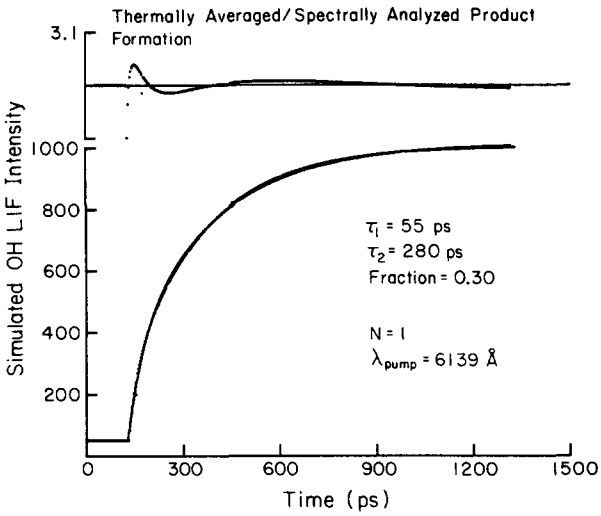

FIG. 10. PST calculation of product yield vs time, including all possible discrete transitions [Eq. (6)]. Excitation wavelength is 6139 Å, probe transition is for $N = 1$. The time scale is such as to facilitate comparison with the experimental results in Fig. 4. The residual, the difference between the data points and the fitting function, shows a damped increasing period oscillation which indicates that the simulated data is composed of more exponential components than just the two of the fitting function. (A linear predictor exponential fitting routine (Ref. 46), courtesy of Dr. M. Rosker, shows that there are approximately five significant components, in this case.) The biexponential model function, however, fits the overall shape of the transient allowing comparison to be made with the experimental data. The calculated transient was convoluted with a simulation of the response function (Ref. 45) to facilitate comparison with the experimental results. This is particularly important for the early time behavior (see the Experimental section).

values and show less correlation. It is expected that PST would yield lifetime results which are faster than the observed values. That the values differ by approximately a factor of 2 might not be surprising in that the transition state is being modeled as very loose. The question of the degree of "flexibility" of the transition state and its effect on the observed behavior (rates and product state distributions) is currently being investigated.[37]

A final remark about the dependence of $P(N,t)$ on N. In realizing the importance of considering discrete transitions for simulation of the experimental results, the question of the influence of the N quantum number on the observed OH product formation may be investigated. Analysis of the kinetics of reaction into the several product channels shows that if a single resonance is excited or reached by energy redistribution, then all products form with the same time constant (see paper I). While the rates are the same, the relative probabilities for the formation of specific product states do vary. In the present study it is not possible to excite a single resonance because of the wide distribution in E and J. The different energy and angular momentum constraints for the formation of the OH product in, e.g., $N = 2$ as compared to $N = 1$, for a distribution of reactant E and J values, changes the number of initial states which may correlate to this product. Such constraints will effect the product yield and the fraction and rates of the product buildup. This is most important in the case of a reaction which proceeds near threshold, it may not be a significant effect for sufficiently large E. Curve 5 of Fig. 9 shows the relative amplitude of the $N = 2$ thermal averaged product formation to be reduced in comparison with the $N = 1$ result. The fitting parameters are the same as curve 4, the exception being that curve 4 was normalized to the same final value (for the plotted range) as curve 1 to facilitate visual comparison.

C. Homogeneous linewidth and IVR: "T_1" and "T_2"

In a molecule with a complex level structure it is important to define the origin of homogeneous broadening in order to interpret the observed spectral results and their impact on predissociation dynamics. A simple model for HOOH, which yields the intrinsic linewidth contributions from the different time-dependent intramolecular processes, can be described as follows. An optically active mode (in this case the OH overtone state ϕ_s) couples to optically inactive bath modes, $\{\phi_l\}$, in the peroxide vibrational/rotational phase space. These states are in turn coupled to the dissociation "continuum" of OH product states (including translational motion). The coherent preparation of the molecular eigenstates (of the Hamiltonian $H = H_0 + V_{sl}$) with a transform limited laser pulse produces the initial zeroth-order state ϕ_s provided the laser bandwidth spans all relevant eigenstates. That is, the initially prepared superposition state in the diagonalized representation is

$$\Psi(0) \equiv \phi_s = \sum_n c_n |\psi_n\rangle,$$

where the ψ_n are the molecular eigenstates with the coefficients c_n. This initial nonstationary state ("packet") will evolve in time, the degree of evolution represented by $|\langle\phi_s|\Psi(t)\rangle|^2$. The time scale for this dephasing is determined by the degree of coupling and the extent of the energy spread of the ψ_n. Following the dephasing, the states evolve by energy relaxation (in this case by predissociation) which leads to a decrease of the HOOH population and concomitant increase in the OH population. This picture is similar to the description advanced for IVR[39] and multiphoton processes, where "T_1" and "T_2" type processes are described.[40] This model was used in paper I[2] to describe the predissociation of NCNO. The HOOH predissociation, however, occurs on the ground state potential energy surface—therefore, only vibrational energy redistribution is required.

With these ideas in mind, it may be understood that the action (or predissociation) spectrum linewidth, which is dominated by inhomogeneous effects, will have a more significant contribution from the dephasing behavior than from the energy relaxation effects. The value of this energy relaxation contribution is the Fourier transform of the rates of reaction measured in these experiments. The linewidth contributions from the dissociation vary from 0.05 to 0.15 cm^{-1} (assuming a Lorentzian line shape), as determined from the fast component of the biexponential buildup. This addition to the linewidth, which is due to population relaxation, is very small compared to the inhomogeneous apparent width of 200 cm^{-1}. Our experiments demonstrate that the OH-stretch overtone band is definitely inhomogeneously broadened to a resolution of $< 10\ cm^{-1}$. Conversely, this gives an upper limit for the homogeneous broadening. These limits

for the inhomogeneous and homogeneous broadenings were established by measuring the rates of OH product appearance as the laser (bandwidth 3 cm^{-1}) was scanned within the main overtone band region (see Fig. 6). The results of a recent study of the action spectrum of jet-cooled HOOH by Butler *et al.*[41] is in agreement with the time-resolved results of Scherer *et al.*[5] in that these jet spectra for the $\Delta v_{OH} = 4$ and $\Delta v_{OH} = 6$ overtone transitions show sharp features which are much narrower than the apparent linewidth for the room temperature spectra.[6] The spectra reported therein show the linewidth (instrument limited) to be approximately 0.08 and 1.5 cm^{-1} for the transitions to the third and fifth overtones, respectively. The contribution of the population relaxation to the linewidth is not determined in their fifth overtone ($\Delta v_{OH} = 6$) results since time-resolved results are not yet available for this state.

The density of states of HOOH near threshold is about 10–200 depending on J. If ten states are effectively involved in the coupling, then the linewidth (due to energy relaxation) and level spacing are comparable. For higher densities the $\{|l\rangle\}$ manifold is essentially a quasicontinuum. This is especially the case considering that the linewidth due to dephasing could be much larger than the 0.05–0.15 cm^{-1} width. (It should be noted that the phase space is not necessarily composed of only a single $|l\rangle$ manifold; a requirement for obtaining nonstatistical behavior is that at least two subspaces are present, as discussed earlier, in Sec. V A 2.) In this limit of fast IVR, the measured picosecond transients give the predissociation rates.

Finally, the inhomogeneous width reported herein for a relatively small molecule might turn out to be general for large molecules. There is some evidence for inhomogeneous contributions to the LM transition in larger systems.[42] Further pump–probe experiments are in progress to obtain energy relaxation and dephasing rates for $v_{OH} = 6$ of HOOH (an other molecular systems) in a molecular beam to further understand the origin of homogeneous line broadening and IVR for high energy LM vibrational states.

VI. CONCLUSIONS

This paper, the second in the series, presents picosecond time-resolved studies of the overtone ($v_{OH} = 5$) initiated unimolecular reaction $HOOH + h\nu \rightarrow 2\,OH(D_0 = 49.6\ kcal\ mol^{-1})$ and provides a detailed account of our previously communicated results.[5] The primary findings reported here are: (a) the measurement of the homogeneous contribution(s) to the linewidth; (b) observation and analysis of quasibiexponential and nonmonotonic in pump wavelength behaviors; and (c) determination of the significant difference in the rate(s) of dissociation for overtone and repulsive state excitation.

(a) The OH local-mode transition to the fourth overtone ($v_{OH} = 5$) is inhomogeneously broadened. The apparent width is observed to be about 200 cm^{-1}, while the predissociation rate contribution to the *homogeneous* width is 0.05–0.15 cm^{-1}. The inhomogeneity of the spectra is evident from the results of picosecond experiments which examined the variation of the transient behavior as a function of the excess vibrational energy (for excitation within the LM absorption band) in HOOH. The homogeneous contribution is determined from real-time measurements of the actual rate of OH product formation. The energy relaxation time (T_1) is 30 to 100 ps while the pure dephasing time (T_2') is $\geqslant$0.5 ps.

(b) The time dependent behavior of OH product formation (for each of the product rotational states studied) is (i) quasibiexponential and (ii) nonmonotonic with respect to the pump laser wavelength. The experimental data is analyzed with two different perspectives in mind. First, the possibility of nonstatistical (non-RRKM) behavior is addressed and related to both of these observations; biexponential and nonmonotonic behaviors. In this case, a divided vibrational phase space is invoked and a simple kinetic model may be used to reproduce the biexponential behavior. Second, the initial thermal distribution and the inhomogenious nature of the spectral transitions within the laser bandwidth are incorporated into an analysis of the present studies. Considering the multitude of discrete transitions possible for a given laser bandwidth facilitates understanding the nonexponential and nonmonotonic behavior of the rates in the predissociation of HOOH at room temperature. Deciding whether these behaviors reflect nonstatistical dynamics or not must await the results of future beam experiments. Such molecular beam studies, similar in spirit to those of papers I and III, should allow for gaining an understanding of the photofragmentation in a state-to-state manner. Such measurements will also allow critical comparisons to be made with statistical theories and with the results obtained from the model calculations of Uzer, Hynes, and Reinhardt and others. Our goal in such experiments is to resolve the different timescales for IVR and predissociation, as discussed in the model given here.

(c) Experiments were performed wherein the OH fragments are produced following UV excitation of the peroxide, instead of reaction initiation by way of overtone (visible) excitation. The results indicate that, in constrast with the 30–100 ps buildup time (depending on pump wavelength) for the overtone predissociation, the UV initiated dissociation of HOOH may be modeled as a single exponential rise of $\leqslant$8 ps. This observation is consistent with the interpretation that the upper potential energy surface, reached via the UV excitation, is directly dissociative–repulsive in nature. These experimental results also provide a way (in addition to the other diagnostic experiments reported herein) to determine that the dynamics observed for the very weak absorption overtone transition are not due to a two-photon pump process.

ACKNOWLEDGMENTS

This research was supported by a grant from the National Science Foundation (CHE-8512887). Some additional support was provided by the Presidential Fund and the Keck Foundation. We thank Professor Rudy Marcus for many useful discussions concerning RRKM theory. We would like to thank Lutfur Khundkar for enlightening conversations regarding statistical theories. We thank Dr. Joseph Perry for his invaluable assistance during the formative period of this project and for his continued interest, and Dr.

Fuad Doany for his help in the initial state of this research. We are also grateful to Professor F. Crim for his help and interest throughout these studies, and Professor J. Troe for communicating results prior to publication. Finally, the early attempts to study overtone dynamics on the picosecond time scale (1981) involved the dedicated efforts and hard work of Mr. Joseph Perry and Dr. Eugene Ryabov, and this must be acknowledged here.

APPENDIX

The direct count method employed considers all of the bound torsional eigenstates, which are evaluated using the torsional potential parameters of Hunt *et al.*[9] and Dubal *et al.*[6] The torsional eigenvalues and eigenvectors are obtained by numerically solving the Schrödinger equation. The values for the terms of the kinetic energy prefactor $\alpha(\chi)$ and the potential $V(\chi)$ are given in Table I for the ground and $v_{OH} = 5$ torsional potentials. The issue of treating the hindered rotor levels above the torsional barrier was not considered here; only the torsional levels up to the (*cis*) barrier height are considered. Moreover, the issue of torsion–rotation interaction was ignored; this has the effect of maintaining the same values for the rotational constants for all states. The two rotational motions related to this prolate near symmetric top's B and C constants were treated as adiabatic rotations, whereby J is a constant of the motion and the K quantum number (the projection of J onto the figure axis) is not. Nuclear spin statistics and the OH $\Omega = \frac{1}{2}$ OH spin–orbit state were not included in the calculation. In our previous paper[5] we incorporated a different direct count algorithm (Hase–Bunker[43]) which gave qualitative agreement with the experimental results (i.e., it gave a biexponential form), but was quantitatively in poorer agreement than the present calculation. Our previous calculation postulated a somewhat tight transition state as opposed to the present calculation which invokes a loose transition state via PST.

Finally, it should be mentioned that the purpose of the present calculation has been to illustrate, in the simplest manner, the comparison between the predictions of standard statistical theories and our experimental results. A more complete theoretical treatment, which includes a modified treatment for the determination of the transition state will be given in Ref. 37.

[1]See for example, K. V. Reddy, D. F. Heller, and M. J. Berry, J. Chem. Phys. **76**, 2814 (1982); K. V. Reddy, R. G. Bray, and M. J. Berry, in *Advances in Laser Chemistry*, edited by A. H. Zewail (Springer, New York, 1978), p. 48.

[2]L. R. Khundkhar, J. L. Knee, and A. H. Zewail, J. Chem. Phys. **87**, 77 (1987), paper I in this series.

[3]See e.g., B. R. Henry, Acc. Chem. Res. **10**, 207 (1977); W. M. Gelbart, P. R. Stannard, and M. L. Elert, Int. J. Quant. Chem. **14**, 703 (1978); H. L. Fang and R. L. Swoford, J. Chem. Phys. **72**, 6382 (1980); M. L. Sage and J. Jortner, Adv. Chem. Phys. **47**, 293 (1981); M. S. Child and L. Halonen, *ibid.* **57**, 1 (1984); E. L. Sibert, W. P. Reinhardt, and J. T. Hynes, J. Chem. Phys. **81**, 1115 (1984).

[4]J. W. Perry and A. H. Zewail, J. Chem. Phys. **70**, 582 (1979); Chem. Phys. Lett. **65**, 31 (1979); J. Phys. Chem. **86**, 5197 (1982); J. Chem. Phys. **80**, 5333 (1984).

[5]N. F. Scherer, F. E. Doany, A. H. Zewail, and J. W. Perry, J. Chem. Phys. **84**, 1932 (1986).

[6(a)]T. F. Rizzo, C. C. Hayden, and F. F. Crim, Faraday Discuss. Chem. Soc. **75**, 223 (1983); T. F. Rizzo, Ph.D. thesis, University of Wisconsin (Madison), 1984. (b) H. R. Dubal and F. F. Crim, J. Chem. Phys. **83**, 3863 (1985); T. M. Ticich, T. R. Rizzo, H. R. Dubal, and F. F. Crim, J. Chem. Phys. **84**, 1508 (1986).

[7]L. T. Molina and M. J. Molina, J. Photochem. **15**, 97 (1981); J. J. Willman, D. F. Jennings, W. B. Olson, and A. Goldman, J. Mol. Spectrosc. **117**, 46 (1986); G. A. Khachkuruzov and I. N. Przhevalskii, Opt. Spectrosc. **36**, 172 (1974); **44**, 112 (1978); P. A. Giguere, J. Chem. Phys. **18**, 88 (1950).

[8]D. Cremer, J. Chem. Phys. **69**, 4440 (1978); R. Block and L. Jansen, *ibid.* **82**, 3322 (1985), and references therein.

[9]E. Hirota, J. Chem. Phys. **28**, 839 (1958); R. L. Redington, W. B. Olson, and P. C. Cross, *ibid.* **36**, 1311 (1962); R. L.Hunt, R. A. Leacock, C. W. Peters, and K. T. Hecht, *ibid.* **42**, 1931 (1965).

[10]G. Ondrey, N. van Veen, and R. Bersohn, J. Chem. Phys. **78**, 3732 (1983); S. Klee, K. Gericke, and F. J. Comes, *ibid.* **85**, 40, 4463 (1986).

[11]E. M. Evleth, J. Am. Chem. Soc. **98**, 1693 (1976).

[12]T. Uzer, J. T. Hynes, and W. P. Reinhardt, Chem. Phys. Lett. **117**, 600 (1985); J. Chem. Phys. **85**, 5791 (1986); see also the work of Ref. 47.

[13]H. Okabe, *Photochemistry of Small Molecules*, (Wiley, New York, 1978).

[14]H. Klann, J. Kuhl, and D. von der Linde, Opt. Commun. **38**, 390 (1981).

[15]A. Yariv, *Quantum Electronics*, 2nd ed. (Wiley, New York, 1975); G. R. Flemming, Adv. Chem. Phys. **49**, 1 (1982), and references therein.

[16]E. P. Ippen and C. V. Shank, in Topics in Applied Physics, edited by S. L. Shapiro (Springer, Berlin, 1977), Vol. 18, p. 83.

[17]D. von der Linde, Appl. Phys. B **39**, 201 (1986).

[18]H. A. Pike and M. Hersher, J. Appl. Phys. **41**, 4562 (1970).

[19]D. P. Millar and A. H. Zewail, Chem. Phys. **72**, 381 (1982); G. R. Flemming Adv. Chem. Phys. **49**, 1 (1982).

[20]J. M. Clemens, J. Najbar, I. Bronstein-Bronte, and R. M. Hochstrasser, Opt. Commun. **47**, 271 (1983).

[21]N. F. Scherer, J. W. Perry, F. E. Doany, and A. H. Zewail, J. Phys. Chem. **89**, 894 (1985).

[22]Y. R. Shen, *The Principles of Nonlinear Optics* (Wiley, New York 1984).

[23]I. S. McDermid and J. B. Laudenslager, J. Chem. Phys. **78**, 1824 (1982); K. H. Gericke and F. J. Comes, Chem. Phys. **65**, 113 (1982).

[24]G. P. Smith and D. R. Crosley, J. Chem. Phys. **85**, 3896 (1986); J. H. Bechtel and R. E. Teets, Appl. Opt. **18**, 4138 (1979).

[25]D. W. Marquardt, J. Soc. Ind. Appl. Math. **11**, 431 (1963); P. R. Bevington, *Data Reduction and Error Analysis for the Physical Sciences*, (McGraw–Hill, New York, 1969); D. P. Millar, Ph.D. thesis, California Institute of Technology, 1982.

[26]A true absorption spectrum, instead of the action spectrum, would be an asset to gaining a complete understanding of the transitions and transition frequencies for $v_{OH} = 4,5,6$.

[27]G. H. Dieke and H. M. Crosswhite, J. Quant. Spectrosc. Radiat. Transfer. **2**, 97 (1962); W. L. Dimpfl and J. L. Kinsey, *ibid.* **21**, 233 (1979); M. Alexander and P. Dagdigian, J. Chem. Phys. **80**, 4325 (1984).

[28]K. Gericke, S. Klee, F. Comes, and R. N. Dixon, J. Chem. Phys. **85**, 4463 (1986); M. P. Docker, A. Hodgson, and J. P. Simons, Chem. Phys. Lett. **128**, 264 (1986); P. Andersen, G. S. Ondrey, and B. Titze, J. Chem. Phys. **80**, 2548 (1984).

[29]See for example, J. A. Silver, W. L. Dimpfl, J. H. Brophy, and J. L. Kinsey, J. Chem. Phys. **65**, 1811 (1976).

[30]It would also be interesting to perform UV excitation experiments at twice the photon energy of that used in the overtone excitation, i.e., about 306 nm.

[31]N. F. Scherer, J. L. Knee, D. D. Smith, and A. H. Zewail, J. Phys. Chem. **89**, 5141 (1985).

[32]See J. W. Perry, N. F. Scherer, and A. H. Zewail, Chem. Phys. Lett. **103**, 1 (1983); L. R. Khundkar, R. A. Marcus, and A. H. Zewail, J. Phys. Chem. **87**, 2473 (1983).

[33]W. L. Hase, J. Phys. Chem. **90**, 365 (1986); R. A. Marcus, J. Chem. Phys. **85**, 5035 (1986).

[34]J. L. Knee, L. R. Khundkar, and A. H. Zewail, J. Chem. Phys. **87**, 115 (1987), paper III in this series.

[35]See paper I for references of RRKM, SACM, PST, and others. Also, we

were informed in a private communication (F. Crim) that the rate of reaction near threshold has a significant dependence on the J quantum number (determined from SACM calculations by Troe's group); work in progress.

[36]See J. O. Hirschfelder, C. F. Curtis, and R. B. Bird, *Molecular Theory of Gases and Liquids* (Wiley, New York, 1954); the value of C_6 was obtained by a similar procedure to that referenced in Ref. 6.

[37]N. F. Scherer, L. R. Khundkar, D. Wardlaw, R. A. Marcus, and A. H. Zewail (work in progress).

[38]The fraction of the amplitude of the fast component to the total amplitude is found to be fluctuating (see Tables II and IV). This may depend on the extent of the rotational energy contribution to the total energy of reaction. Additionally, Table IV shows that the contribution of vibrational energy to the total energy is the smallest near 6134 Å and largest neart 6160 Å (see the text and Ref. 6).

[39]P. M. Felker and A. H. Zewail, J. Chem. Phys. **82**, 2961, 2975, 2994 (1985).

[40]See e.g., N. Bloembergen and A. H. Zewail, J. Phys. Chem. **88**, 5459 (1984).

[41]L. J. Butler, T. M. Ticich, M. D. Likar, and F. F. Crim, J. Chem. Phys. **85**, 2331 (1986).

[42]M. C. Chung and R. N. Zare, J. Chem. Phys. **82**, 4791 (1985).

[43]W. L. Hase and D. L. Bunker, program QCPE-234, Caltech, Pasadena, CA 91125.

[44]D. M. Wardlaw and R. A. Marcus, J. Chem. Phys. **83**, 3462 (1985).

[45]The calculated transients, of the form $P(N,t)$, Eq. (6), are convoluted with a Gaussian pulse to produce transients for comparison with the experimental results. The procedure is similar to that of Eq. (1) except that the transients here are rising exponentials.

[46]H. Barkhuijsen, R. DeBeer, W. M. M. J. Bovee, and D. Van Ormonolt, J. Magn. Reson. **61**, 465 (1985).

[47]B. G. Sumpter and D. L. Thompson, J. Chem. Phys. **86**, 2805 (1987); John S. Hutchinson, *ibid.* **85**, 7087 (1986), and references therein.